Lowry, O. H., Rosebrough, N. J., Farr, A. L., & Randall, R. J. (1951) *J. Biol. Chem. 193*, 265-275.
Maurer, A., McIntyre, J. O., Churchill, S., & Flesicher, S. (1985) *J. Biol. Chem. 260*, 1661-1669.
Moras, D., Olsen, K. W., Sabesan, M. N., Buehner, M., Ford, G. C., & Rossman, M. G. (1975) *J. Biol. Chem. 250*, 9137-9162.
Peterson, G. L. (1977) *Anal. Biochem. 83*, 346-356.
Phelps, D. C., & Hatefi, Y. (1981a) *Biochemistry 20*, 453-458.
Phelps, D. C., & Hatefi, Y. (1981b) *Biochemistry 20*, 459-463.
Prasad, P. V., & Hatefi, Y. (1986) *Biochemistry 25*, 2459-2464.
Rossman, M. G., Liljas, A., Branden, C.-I., & Banaszak, L. J. (1975) *Enzymes (3rd Ed.) 11*, 61-102.
Schott, H., Rudloff, E., Schmidt, P., Roychoudhury, R., & Kossel, H. (1973) *Biochemistry 12*, 932-938.
Yamaguchi, M., Chen, S., & Hatefi, Y. (1985) *Biochemistry 24*, 4912-4916.

Restrained Refinement of the Monoclinic Form of Yeast Phenylalanine Transfer RNA. Temperature Factors and Dynamics, Coordinated Waters, and Base-Pair Propeller Twist Angles†

E. Westhof
Institut de Biologie Moleculaire et Cellulaire, Centre National de la Recherche Scientifique, F-67084 Strasbourg Cedex, France
M. Sundaralingam*
Department of Biochemistry, College of Agricultural and Life Sciences, University of Wisconsin, Madison, Wisconsin 53706
Received December 18, 1985; Revised Manuscript Received April 25, 1986

ABSTRACT: The structure of yeast phenylalanine transfer RNA in the monoclinic form has been further refined by using the restrained least-squares method of Hendrickson and Konnert. For the 4019 reflections between 10 and 3 Å, with magnitudes at least 3 times their standard deviations, the *R* factor is 16.8%. The variation of the atomic temperature factors along the sequence indicates that the major flexibility regions are the amino acid and anticodon stems. The two strands of the amino acid helix exhibit large differential temperature factors, suggesting partial uncoiling or melting of the helix. In this work, the occupancy of all atoms was also varied. Residues D16 and D17 of the dihydrouridine loop as well as U33 and G37 of the anticodon loop have occupancies around 70%, indicating some local disorder or large-scale mobility at these positions. One hundred fifteen solvent molecules, including five magnesium ions, were found in difference maps. The role of several water molecules is clearly related to the stabilization of the secondary and tertiary interactions. The gold sites, which were not previously discussed, are described and show an energetically favored binding mode similar to that of cobalt and nickel complexes with nucleotides.

Yeast phenylalanine transfer RNA (tRNA) crystallizes in two forms: monoclinic (Ichikawa & Sundaralingam, 1972; Ladner et al., 1972) and orthorhombic (Kim et al., 1971). Both are closely related forms with similar unit cell dimensions for the *a* and *b* axes (56.3 and 33.4 Å, respectively) while the *c* axis is about 2.5 times shorter in the monoclinic (63.0 Å) than in the orthorhombic (161.6 Å). The orthorhombic form has been refined with the program COREL S (Sussman et al., 1977) to 19.8% with individual atomic temperature factors or to 23.1% with group temperature factors for 8426 data up to 2.7-Å resolution (Sussman et al., 1978). The monoclinic form was refined by the MRC group using the Jack–Levitt refinement method (Jack & Levitt, 1978) to an *R* factor of 21% for 8006 data up to 2.5-Å resolution (Hingerty et al., 1978). The Madison group refined the monoclinic form using 6542 data up to 2.7 Å with difference Fourier methods down to 31.2% (Stout et al., 1978). Here, we report further refinement studies on the monoclinic form using the restrained refinement method of Hendrickson and Konnert (1980). This new refinement was performed in order to remove from the comparisons, between the structures of transfer RNA molecules known at high resolution, artifacts that might be introduced by different refinement methods. Extensive and precise comparisons between transfer RNA molecules are called for in view of the recent results obtained with yeast tRNA-Asp (Moras et al., 1985; Westhof et al., 1985). These results suggest that the structure of yeast $tRNA^{Asp}$ is a model for a tRNA molecule bound to a messenger codon triplet while that of yeast $tRNA^{Phe}$ is a model for the unbound tRNA molecule. This interesting observation has led to specific concern about the effects of crystallization conditions and of crystalline packing on temperature factors and dynamics. The results of the present refinement offer new insights on the yeast $tRNA^{Phe}$ molecule, and those will be principally discussed in this report.

Experimental Procedures

Data Collection and Refinement. The data used in this work were collected on a CAD4 diffractometer (Stout et al., 1978). The data were scanned out to 2.7 Å, and 8300 reflections were measured. Of these, 4019 reflections between 10 and 3 Å were above the 3σ level, and these were used in the present structure refinement.

The structure was refined by using the Konnert–Hendrickson restrained program (Hendrickson & Konnert, 1980;

† M.S. gratefully thanks the National Institutes of Health for Grant GM 18455.

0006-2960/86/0425-4868$01.50/0

Table I: Summary of Refinement Parameters

mean F_{obsd}	284.1
mean $(F_{obsd} - F_{calcd})$	47.8
$(F_{obsd} - F_{calcd})/F_{obsd}$	0.168
final σ applied on F_{obsd}	40.0
σ/F_{obsd}	0.141
mean positional shift (Å)	0.012
mean thermal shift (Å^2)	0.15
R factor[a]	0.168
correlation coefficient between F_{obsd} and F_{calcd}[a]	0.93
$K = \sum F_{obsd}/\sum F_{calcd}$	1.022
resolution range (Å)	10.0–3.0
no. of reflections	4019
no. of parameters	7069
ratio of observations to parameters	0.6
no. of tRNA atoms	1652
no. of solvent atoms	115
mean thermal factor (Å^2)	20.5

[a] The R factor is defined as $\sum|F_{obsd} - F_{calcd}|/\sum|F_{obsd}|$. The correlation coefficient is given by the expression $\sum[(F_{obsd} - \bar{F}_{obsd})(F_{calcd} - \bar{F}_{calcd})]/[\sum(F_{obsd} - \bar{F}_{obsd})^2\sum(F_{calcd} - \bar{F}_{calcd})^2]^{1/2}$.

Konnert & Hendrickson, 1980) modified for nucleic acids, NUCLSQ (Westhof et al., 1985). In this program, the nucleic acid geometry is restrained to standard values obtained from small molecule crystallography within some σ value. Special care is attached to the restraints of the sugar puckers because of the central importance of the sugar in the polynucleotide chain (Sundaralingam, 1969, 1973). This is accomplished by "ad hoc" restraints on chiral volumes centered on each furanose ring atom (Westhof & Sundaralingam, 1983; Westhof et al., 1985).

Coordinates for the monoclinic form were available from our previous work (Stout et al., 1978) and from the MRC studies (Hingerty et al., 1978). The correspondence between these two coordinate sets is generally good. As the coordinates for the MRC structure are the result of more extensive refinement, these were used as starting coordinates in the present refinement with our data.

In the Hendrickson–Konnert method, the difference between observed and calculated structure factors is minimized by least squares together with additional quantities that involve the sum of the differences between the ideal and model geometries. The structure factor term is weighted by the inverse of the square of $(F_{obsd} - F_{calcd})$. For each geometrical term, the weight is given by the inverse of the square of σ with the σ values corresponding to the known spread of each geometrical term in small-molecule crystallography. The σ values used are given in Table S-I (in the supplementary material; see paragraph at end of paper regarding supplementary material) together with the root mean square (rms) deviation from ideality at the end of the refinement. The statistics of the refinement are given in Table I.

At several steps of the refinement, electron density and difference Fourier maps were scrutinized with the graphics program FRODO (Jones, 1982). The peaks obtained after the difference Fourier maps were scanned for contacts with the tRNA molecule with a program written by S. T. Rao (University of Wisconsin). The solvent peaks were then introduced in the refinement for three cycles with unit occupancy and variable temperature factors. Afterward, the refinement was continued with three cycles with constant temperature factor and variable occupancy for the solvent atoms. New difference maps were then calculated and the overall cycles of refinement pursued until no meaningful residual peaks could be found in the maps.

The rms value between the coordinates of the MRC refinement (Hingerty et al., 1978) and those of the present refinement is 0.48 Å, while that between the coordinates of the yeast tRNA^{Phe} in the orthorhombic form (Sussman et al., 1978) and those of the present refinement is 0.78 Å. The highest displacements (about 1.0 Å in the former comparison and 1.5 Å in the latter) are among the terminal residues of the amino acid stems (and the terminal A76) and the anticodon loop residues (35–37). The deviations of the backbone phosphates between our refined monoclinic tRNA, the MRC monoclinic model (Hingerty et al, 1978), and the orthorhombic model (Sussman et al., 1977) are shown in Figure S-1 (in the supplementary material).

Results and Discussion

The Structure. The L-shaped tRNA structure is composed of four helical stems, which are stacked in pairs one on top of the other and linked together by single-stranded loops and stretches. None of these four stems are self-complementary helices. In the first approximation, the four helices can be regarded as independent structures of oligoribonucleotides. The amino acid (AA) stem is a heptaribonucleotide helix, while the thymine (T) and anticodon (AC) stems are both pentanucleotide helices. The tetranucleotide D helix is expected to be perturbed by the numerous tertiary interactions including base triples in the broad groove of the helix, while the other helices are independent of such interactions. Therefore, the latter helices provide insights on the structural properties of RNA helices. This is important in view of the fact that tRNAs are the only structures known to date that provide such information. In contrast, for DNA, deoxyribonucleotide helical fragments are providing information on the helical properties, base pair geometries, and nucleotide conformations.

The base-pair twist, propellar twist, and roll angles [as defined by Fratini et al. (1982)] for the various base pairs in the helical stems, calculated with two different programs, are given in Table II. The values for the twist and propellar twist obtained with the two programs are in good agreement. However, those for the tilt and the roll do not compare well. The latter values are very sensitive to the method of calculation. While the average twist angle between base pairs is close to the value, 32.7°, determined by fiber diffraction, the average rise per residue, 2.5 Å, is significantly less than in RNA-11, 2.81 Å (Arnott et al., 1973). This was already noted previously (Jack et al., 1976; Holbrook et al., 1978). It is interesting, however, to remark that the average rise per residue in the structures of deoxyoligomers in the A form (Jurnak & McPherson, 1985), 2.82 Å, is the RNA-11 value. This observation implies that the hydrogen bond between the ribosyl O(2′) atom of one residue and the furanose O(4′) atom of the next helical residue (see Table S-III) is partly responsible for the different helical rises in tRNA and RNA fibers, besides the different environments of the helices (Jack et al., 1976). From Table II, it is apparent that the twist angles and the propeller twist of the base pairs show large variations from one base pair to the other. Interestingly, the G-C base pairs seem to assume larger propeller twist angles than the A-U base pairs in this structure. Note the very large twist (43.9°) of the base pair G3-C70 stacked over the wobble base pair G4-U69. In contrast, in yeast tRNA^{Asp} (Westhof et al., 1985), a very large twis (40.5°) is observed for the wobble base pair U5-G68 with the base pair below G6-C67. This follows from the fact that, in yeast tRNA^{Phe}, the wobble pair is a 5′-end G-U pair with interstrand stacking with the preceding pair, while it is the other way around in yeast tRNA^{Asp} (Mizuno & Sundaralingam, 1978).

In Figure S-2 are shown the propeller twist angles for the base pairs of the anticodon, amino acid, and thymin stems

Table II: Parameters of Local Geometry in the Various Stems of Yeast $tRNA^{Phe}$ [a,b]

	propeller twist (deg)	twist (deg)	tilt (deg)	roll (deg)
		Amino Acid Stem		
G1-C72	8.2/6.3	25.9/27.9	−9.1/−3.0	3.9/2.3
C2-G71	7.2/8.4	25.8/30.0	9.3/6.2	−9.0/−8.1
G3-C70	9.5/8.9	43.9/40.6	−11.3/−0.6	−9.0/−13.9
G4-U69	16.0/12.9	26.3/29.9	8.9/0.0	−9.6/−7.8
A5-U68	12.0/12.5	29.3/32.1	0.3/3.5	−4.7/−2.0
U6-A67	19.7/17.7	31.8/33.6	3.7/2.6	−16.5/−15.4
U7-A66	4.5/5.2			
av	11.0/10.3	30.5/32.3	0.3/0.6	−7.5/−7.5
		Dihydrouridine Stem		
G10-C25	14.9/15.0	39.1/41.4	−7.2/0.3	−5.2/−10.0
C11-G24	25.5/24.9	34.6/35.5	−5.1/−1.0	−10.4/−10.7
U12-A23	7.1/5.9	25.8/27.1	5.2/3.6	0.6/0.0
C13-G22	15.6/14.6			
av	15.7/15.1	33.2/34.7	−2.4/1.0	−5.0/−10.3
		Anticodon Stem		
G26-A44	36.8/31.6	40.0/40.8	−17.4/3.2	−5.3/23.3
C27-G43	20.1/20.1	26.7/28.5	1.6/1.3	−1.6/3.7
C28-G42	13.0/14.4	34.1/34.2	−5.2/−7.7	11.7/11.2
A29-U41	7.3/8.1	33.6/37.6	0.6/1.3	−2.7/0.8
G30-C40	21.5/19.9	29.7/31.2	−6.5/4.6	−2.5/0.2
A31-39	11.6/17.7			
av with G26-A44	18.4/18.6	32.8/34.5	−5.4/0.5	−0.2/7.8
av without G26-A44	14.7/16.0	31.0/32.9	−2.4/−0.1	1.2/4.0
		Thymine Stem		
C49-G65	16.2/14.8	32.3/33.6	−4.3/1.7	−1.9/−3.4
U50-A64	10.2/10.4	34.0/34.4	−1.2/2.9	10.9/−12.3
G51-C63	15.6/16.6	29.3/30.7	−1.9/−1.9	5.9/−7.4
U52-A62	10.8/11.2	31.8/32.8	1.1/1.8	−5.6/−4.9
G53-C61	25.1/19.8			
av	15.6/15.3	31.9/32.9	−1.6/1.1	2.3/−7.0
		Av over Stems (without G26-A44)		
	14.3/14.2	32.1/33.2	−1.5/0.6	−2.2/−5.2
		Av Propeller Twist		
G-C pairs (all)	16.0/15.3			
G-C pairs (without AA stem)	18.6/17.8			
A-U pairs (all)	10.4/10.1			
A-U pairs (without AA stem)	9.4/8.9			

[a] First values were calculated with a program written by W. K. Olson and second values with a program written by J. Rosenberg and R. Dickerson. In the first program, the long axis of a base pair is drawn from N9 (Pur) and N1 (Pyr), the z axis of a base pair is chosen as the mean of the normals to the two bases, and the y axis is chosen to form a right-handed system. The origin of the base-pair coordinate frame is positioned at one of the glycosyl nitrogens. The second program is described in Fratini et al. (1982). [b] Average rise per residue is 2.5, 2.5, 2.2, and 2.5 Å, respectively, for the amino acid, dihydrouridine, anticodon, and thymine stems.

before and after the inclusion of water molecules. The propeller twist angles generally show higher values for the case with water molecules. It is clear that the interactions between water molecules and hydrophilic atoms on the base could distort the local base-pair geometry. We do not know, however, whether those differences are genuine and real or a measure of the error in the positioning of the base planes and the determination of propeller twist angles. The twist angles are on the other hand much less influenced by the presence of water molecules in the refinement.

Temperature Factors and Dynamics of tRNA. The group-average temperature factors for the individual residues are given in Table III and Figure 1. A marked feature is that the AA stem end and the AC loop and AC stem show the highest temperature factors besides a few residues in the D loop (16 and 17), in the T loop (59 and 60), and in the V loop (47). The same trends were noted by Sussman et al. (1978), although the magnitudes of the temperature factors they determined were much higher. All of the residues (16, 17, 59, 60, 47) with high temperature factors are located in looped-out regions and are therefore expected to exhibit high thermal motion. Similarly, the parts of the AA stem and the AC loop with high temperature factors are furthermost removed from the center of gravity of the molecule and are expected to display large thermal motions. The phosphates do not have systematically higher temperature factors than the bases even in the helical stems; for example, all phosphates of the D stem have lower temperature factors than their bases. Similarly, in the loops, the bases do not always have higher temperature factors than their phosphates; for example, the phosphates of A14 and Y37 have higher temperature factors than their corresponding bases. If real, these effects should reflect the interactions made either by the base or by the phosphate and the local dynamics. But, up to now, only some of those effects can be explained on the basis of local interactions.

With the exception of the 3′-ACCA-end which exhibits some disorder, the AA stem and AC helix do not show any evidence of disorder. Thus, the thermal motion parameters are a correct reflection of the dynamics of the molecule. However, in the case of the D and V loops, it is entirely possible that the thermal motion also includes some component of statistical disorder. This is reflected in the occupancy parameter of some of these residues, for example, 16 (see below). An interesting feature that is observed for the temperature factors of the AA stem is that the 5′-end chain shows much larger temperature factors than the corresponding 3′-end chain, with the largest difference (24.5 Å) being observed at the G4-U69 wobble base pair. It is not clear why this is so, although the -ACCA attachment to the 3′-chain may dampen the motion of the 3′-end. This differential motion of the chains is not as pronounced for the AC helix and is not seen in the T helix. These helices are tethered by a hairpin loop in contrast to the AA stem. In yeast $tRNA^{Asp}$, where the -CCA end is completely disordered, no such differential motion is seen between the 3′- and 5′-end chains of the AA stem. The A-U base pairs at the base of the AA stem in the monoclinic form of yeast $tRNA^{Phe}$ are found to show rather high temperature factors.

A possible explanation for the large differential temperature factors of the two chains is that the base pairs of the AA helix are exhibiting some "breathing" with the 5′-strand starting to uncoil. The G4-U69 "wobble" pair in the middle of the AA stem may influence the "uncoiling" of the 5′-strand in two respects. First, G-U pairs induce a deviation in the helical geometry at the level of the phosphate of G and the base of U. A comparison between both strands of the AA helix and a regular RNA-11 helical strand (Arnott et al., 1973) clearly shows that the phosphate of the guanine departs more, and the sugar of the uridine less, from the standard helical position. Indeed, while the phosphorus atom of G4 deviates more than that of U69 (0.56 vs. 0.43 Å), the C(1′) atom of the sugar bound to G4 deviates less than that of U69 (0.07 vs. 0.61 Å). Interestingly, temperature factors reflect those differences: the phosphate of G4 has a temperature factor higher than the base of G4, while the base of U69 has a higher temperature factor than its phosphate. Second, guanine phosphates of G-U pairs have a tendency to adopt the trans conformation about the P–O(5′) and C(4′)–C(5′) bonds instead of the usual gauche⁻

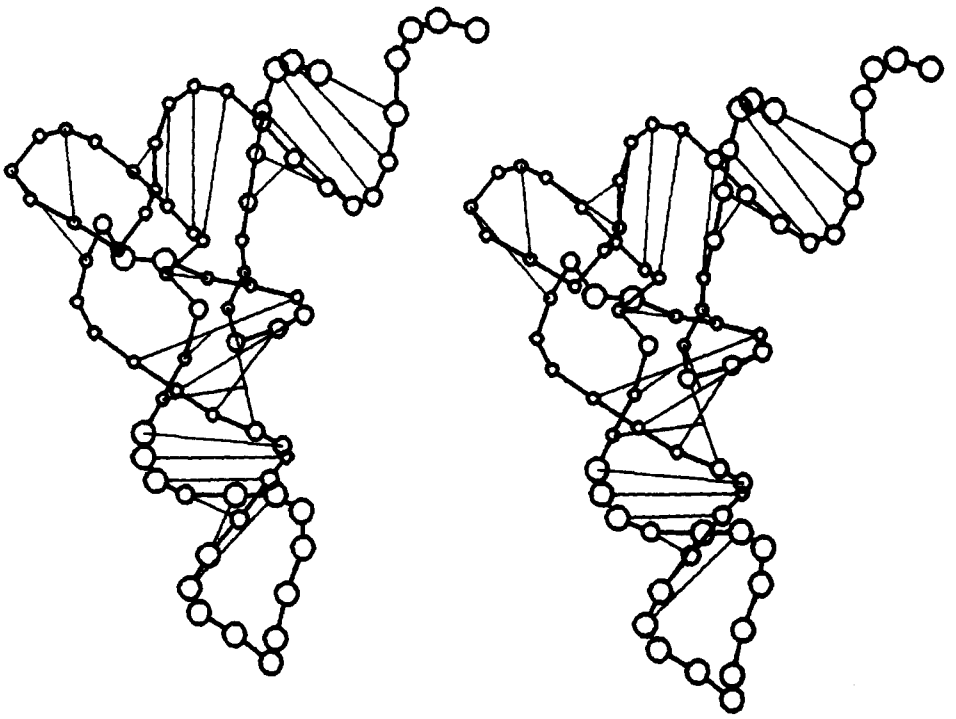

FIGURE 1: Stereoview of the phosphate backbone of tRNA where the radius of each phosphate center is proportional to the average temperature factor for the base, sugar, and phosphate of the nucleotide residue. The larger temperature factors (35–50 Å^2) are found in the -CCA end, the amino acid and anticodon regions, and the looped-out segments of the dihydrouridine loop. The smaller temperature factors (10–20 Å^2) are generally found in the interior of the molecule including the pseudouridine stem and loop.

and gauche$^+$ conformations, respectively, for these bonds (Westhof et al., 1985). Such a conformation exposes the anionic phosphate oxygen atoms to the exterior. This feature of G-U pairs coupled to their dynamics could make them important in tRNA–protein interactions (Ladner et al., 1975; Westhof et al., 1985). It has been shown that the G4-U69 pair is the most readily melting part of the secondary structure of yeast tRNA^{Phe} (Rhodes, 1977). It is interesting that the most frequent positions of G-U pairs in tRNAs are in the AA arm with the guanine base more often on the 5′-strand than on the 3′-strand.

Although atomic temperature factors and occupancies are correlated, these two variables do not correspond to the same physical phenomena. While the occupancy takes care of positional minima separated in conformational space, Debye–Waller factors are most appropriate for local flexibility in a broad minimum of conformational space. Therefore, the structure was refined by varying the occupancy of all atoms. The occupancy of most residues converged to values very close to unity. However, some of the residues had occupancies less than unity (Table IV). As expected, the first and last residues are found among them. The two dihydrouridine residues of the D loop present an interesting situation: the base of D16 and the ribose of D17 have low occupancies, while the base of D17 and the ribose of D16 have not. The same result was obtained in the refinement of yeast tRNA^{Phe} in the orthorhombic form (unpublished results), implying that it cannot be an artifact of the refinement. The position of D16 is different in the two crystalline forms with the base D16 turned toward the inside in the monoclinic form and toward the outside in the orthorhombic form. Thus, the dihydrouridine base could be disordered between the two positions in both crystals. Cleavage of the sugar–phosphate backbone between D16 and D17 (Wintermeyer & Zachau, 1973; Sussman et al., 1978) might contribute also to the low occupancies of these residues. In the anticodon loop, the sugar–phosphate backbone around U33 and Y37 has low occupancy. For U33, the situation was the same in the orthorhombic form but not for Y37, in which case it could be from the different packing. In the structure of yeast tRNA^{Asp} (Westhof et al., 1985), U33 presented also an occupancy less than unity. Thus, it would appear that some large-scale mobility (i.e., not taken care of by temperature factors) is present at D16 and U33 in transfer RNA molecules.

Conformational Torsion Angles. The conformational torsion angles are given in Table S-II. For the C(3′)-endo sugars, Table S-II gives also the mean values (with rms) of the torsion angles together with those for the monoclinic form of yeast tRNA^{Phe} refined by Hingerty et al. (1978). Both sets of mean values are very similar. The rms values are also similar, except for those concerning the sugar pucker. In the present refinement, special care was taken to guarantee proper treatment of sugar puckers, and the sugar pucker restraints are probably slightly too severe. The lack of high-resolution data did not allow the use of less stringent restraints on the sugar puckers. In Figure 2 some important torsion angles are plotted for residues belonging to helical stems (squares) and for residues not belonging to helical stems (crosses). The great majority of residues occupy the preferred domains for the torsions about the P–O(3′) and P–O(5′) bonds (gauche$^-$) and for the torsion about the C(4′)–C(5′) bonds (gauche$^+$) (Sundaralingam, 1969, 1973). Most of the residues outside those conformational ranges do not belong to helical stems, except for the five residues G4, G10, C13, G22, and C49. The residue G4 occurs in the middle of a helical stem but belongs to a wobble G-U pair so that departure from the standard helical sugar–phosphate backbone can be expected (see above). Of the other four residues, G10, G22, and C49 are entering a helical stem and C13 is leaving a helix. Again, nonhelical conformations for the sugar–phosphate backbone are expected in such cases.

The sugars mostly adopt the C(3′)-endo conformation. The twelve residues in the C(2′)-endo conformation are all in single-stranded loops and stretches and cluster in the corner of the molecule that has the highest concentration of tertiary

Table III: Group Average Temperature Factors (Å²)

residue	phosphate	ribose	base	
G1	51.12	35.53	32.66	
C2	43.65	37.63	37.18	
G3	37.32	37.87	35.92	
G4	38.55	23.18	24.26	amino acid stem
A5	23.46	20.71	24.55	
U6	18.35	17.21	20.11	
U7	10.42	3.90	4.48	
U8	5.60	3.51	4.30	
A9	2.10	1.36	6.66	
m2G10	9.03	15.98	20.13	
C11	15.16	15.40	17.36	dihydrouridine stem
U12	14.76	8.24	18.90	
C13	10.52	11.06	11.13	
A14	18.08	5.02	6.59	
G15	3.88	4.02	3.90	
D16	15.59	36.57	38.71	
D17	35.66	27.79	30.11	dihydrouridine loop
G18	15.85	17.09	20.32	
G19	3.45	2.40	6.01	
G20	1.71	3.87	4.35	
A21	5.82	7.73	8.88	
G22	5.33	6.53	12.84	
A23	2.84	5.10	11.46	dihydrouridine stem
G24	13.01	17.52	14.38	
C25	19.82	24.87	29.03	
m22G26	22.07	23.53	19.31	
C27	22.13	17.91	13.85	
C28	23.02	23.62	22.46	
A29	32.73	27.09	24.06	anticodon stem
G30	28.47	29.91	32.98	
A31	34.38	31.62	34.26	
Cm32	24.75	28.27	31.56	
U33	31.38	38.95	41.58	
Gm34	36.18	33.79	31.46	
A35	37.26	36.01	32.44	anticodon loop
A36	40.57	36.63	36.12	
Y37	43.35	34.63	32.59	
A38	39.18	29.70	31.07	
P39	28.68	33.58	34.28	
m5C40	36.56	33.83	33.44	
U41	36.02	26.62	24.04	anticodon stem
G42	25.59	24.51	28.16	
G43	22.12	25.13	28.70	
A44	28.20	24.89	30.71	
G45	28.56	17.67	15.24	
m7G46	16.35	11.04	8.11	variable loop
U47	17.39	26.52	26.53	
C48	12.64	9.30	14.84	
m5C49	18.63	7.18	7.94	
U50	8.84	9.27	10.83	
G51	6.10	4.00	4.25	thymine stem
U52	3.93	9.26	8.91	
G53	6.66	4.71	15.08	
T54	11.39	7.43	6.29	
P55	6.33	11.49	14.44	
C56	7.22	1.10	1.67	
G57	2.98	4.74	10.75	thymine loop
m1A58	2.41	3.33	2.19	
U59	13.97	11.05	15.47	
C60	8.51	7.44	11.80	
C61	10.34	9.85	10.51	
A62	8.68	12.47	5.14	
C63	5.39	7.40	7.15	thymine stem
A64	9.67	8.41	10.30	
G65	14.74	8.78	9.54	
A66	17.81	22.71	18.40	
A67	23.76	21.57	20.26	
U68	19.94	18.26	22.90	
U69	12.68	15.23	23.47	amino acid stem
C70	19.39	19.97	25.79	
G71	22.55	24.94	25.01	
C72	33.26	31.27	30.81	
A73	32.53	32.58	29.66	
C74	38.38	33.89	38.00	
C75	36.55	32.29	29.15	
A76	37.15	36.72	39.49	
av	20.11	18.84	20.13	

Table IV: Residues with Occupancies Less than Unity

residue	group	occupancy
1	phosphate	0.79
16	phosphate	0.99
	ribose	0.94
	base	0.68
17	phosphate	0.95
	ribose	0.67
33	phosphate	0.96
	ribose	0.74
37	phosphate	0.80
	ribose	0.75
76	phosphate	0.93
	ribose	0.93
	base	0.59

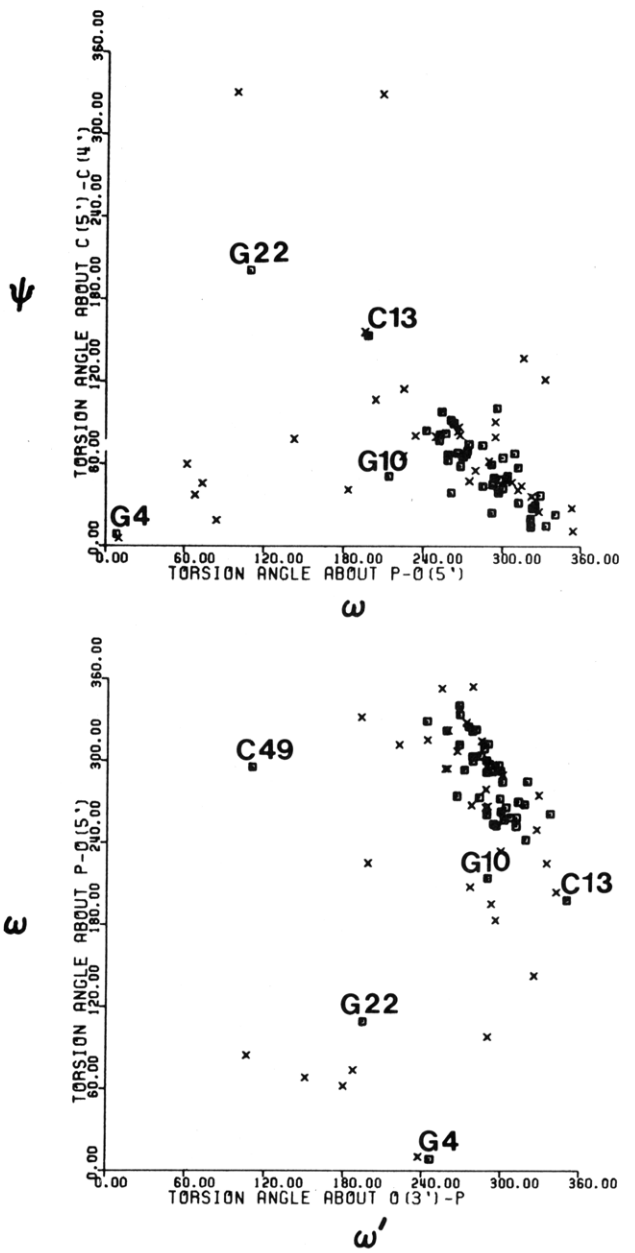

FIGURE 2: For each residue, plot of the torsion angle about C(4′)–C(5′) vs. the torsion angle about P–O(5′) (top) and plot of the torsion angle aboout P–O(5′) vs. the torsion angle about P–O(3′) of the preceding residue (bottom). Residues in helical stems are represented as squares and those outside helical stems as crosses.

interactions and the lowest temperature factors (Figure S-3).

Intramolecular Contacts. A list of intramolecular contacts is presented in Table S-III. Although there are some short contacts, they are within the error on atomic positions. Some

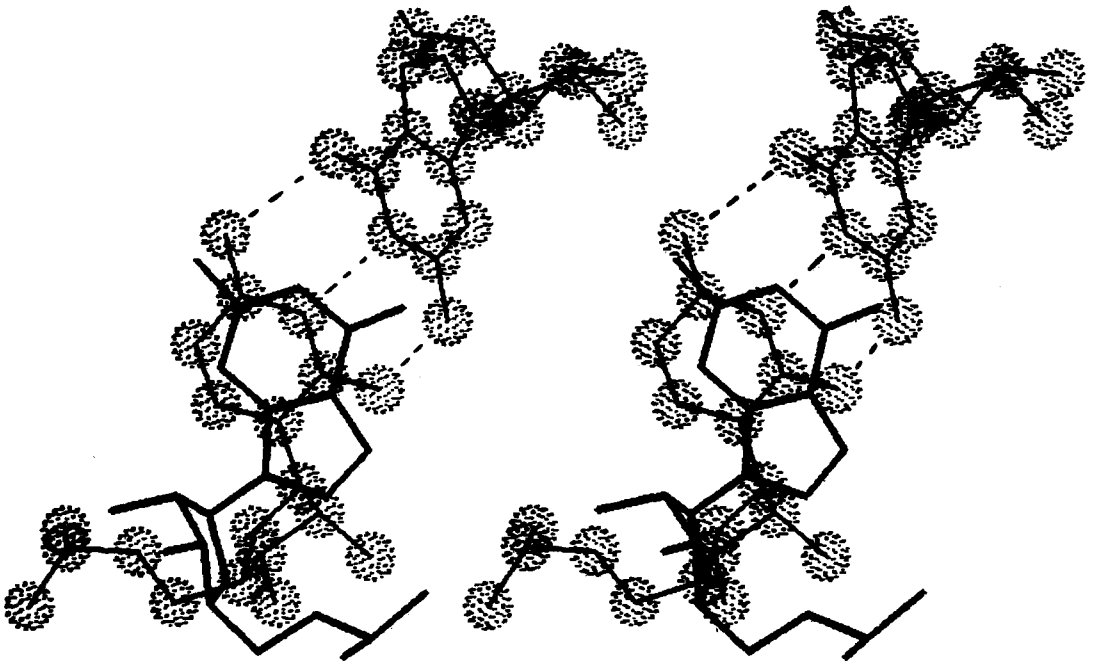

FIGURE 3: Stereoview of the stacking of G20 with C56 of a neighboring molecule which interacts with G19 of the D loop.

interesting contacts are shown in Figures S-4 and S-5. The interaction between the reversed Hoogsteen U8-A14 pair and A21 is different in yeast tRNA^{Asp} (Westhof et al., 1985) from that shown in Figure S-4 (top) where the N1 of the adenine A21 hydrogen bonds to the O(2′) of the residue U8. In tRNA^{Asp}, the adenine A21 has rotated away from U8 toward A14 so that N3 of A21 interacts with N6 of A14 and the O(2′) of A21 with N1 of A14 with only a long interaction between N1 of A21 and the O(2′) of U8.

Most of the tertiary interactions occur between the major groove of the dihydrouridine helix and the stretches U8-A9 (Figure S-4, bottom) and G45-G46. Except for the one-hydrogen-bonded interaction between G45 and G10, the other base–base interactions occur between the bases G22 and A23 of one strand and G46 and A9, respectively. However, several contacts are present between the U8-A9 sugar–phosphate backbone and the bases of the other strand (G10, C11, and C13). These contacts are shown in Figure S-4 (bottom).

The interactions between the D and T loops are also of interest. Figure S-5 (top) shows how G57 of the thymine loop is anchored between the guanines G18 and G19 of the dihydrouridine loop. In addition, there are water molecules on both sides of G57 linking it to G18, G19, and C56. Again, besides base stacking and base pairing, hydrogen bonding between bases and the sugar–phosphate is manifest. On Figure S-5 (top) is also apparent the propeller twist of the tertiary base pair G19-C56. The importance of the interactions to and between the sugar–phosphate backbone is exemplified by the bottom drawing of Figure S-5 where an anionic oxygen of the phosphate of C60 hydrogen bonds to the O(2′) of G58 and to the N4 of C61. Those contacts have been previously described (Ladner et al., 1975; Quigley & Rich, 1976; Goddard, 1977).

Intermolecular Contacts. The number of intermolecular contacts is small (see Table V). This is in sharp contrast to the numerous contacts observed in the structure of yeast tRNA^{Asp} (Westhof et al., 1985). The terminal C75 and A76 bases interact with the minor groove of the AC stem, and a couple of short contacts occur. Those interactions were not restrained and give a measure of the error in the contacts. There is good stacking interaction beween G20 and C56 of neighboring molecules (Figure 3). Also, the anticodon triplet G34-A35-A36 is on top of the minor groove of the T stem; specifically, G34 is in van der Waals contact with the sugar–phosphate backbone of A62-C63. This kind of stacking between a sugar and a neighboring base has been observed in yeast tRNA^{Asp} (Westhof et al., 1985) and in a deoxyoligomer in the A form (Shakked et al., 1983).

Table V: Intermolecular Contacts

atom 1	res[c]	atom 2	res[c]	code[a]	distance (Å)
		Short Contacts (<2.6 Å)			
N2	42	C5′	76	2; 1,0,1	2.5
N3	42	C5′	76	2; 1,0,1	2.1
N2	42	O3′	75	2; 1,0,1	2.5
N2	43	O2	75	2; 1,0,1	2.3
		Hydrogen Bonding Distances (2.6–3.15 Å)			
O2′	5	O2P	53	1; 0,−1,0	3.2
N9	20	O4′	56	2; 2,−1,1	2.8[b]
C8	20	O4′	56	2; 2,−1,1	3.0[b]
O2′	29	O1P	76	2; 1,0,1	2.9
O2′	42	O3′	76	2; 1,0,1	2.6
O2′	43	O2′	75	2; 1,0,1	2.8
		Possible Hydrogen Bonds (3.15–3.45 Å)			
C8	34	O2′	62	1; 0,−1,−1	3.3

[a] The symmetry operation to be applied on the second atom. The first number refers to one of the transformations below and the three subsequent numbers to the translation along x, y, z. (1) x, y, z; (2) $-x$, $y + 0.5$, $-z$. [b] Contacts involving stacking interaction instead of hydrogen bonding. [c] res, residue.

Solvent Binding Sites. One hundred fifteen solvent sites (including five hydrated magnesium ions) were detected in difference maps. Normally, the sites ascribed to water molecules have to be taken with caution. However, similar refinements on the orthorhombic yeast tRNA^{Phe} and yeast tRNA^{Asp} have revealed water molecules in identical environments (unpublished results). Therefore, although some assignments might be incorrect, we think that a majority of the water sites are meaningful. Besides, an analysis of the sites shows that the role of several water molecules is clearly related to a stabilization of the secondary and tertiary interactions.

Figure 4a illustrates a repeated pattern of water–RNA interaction: water molecules bridging the hydroxyl oxygen

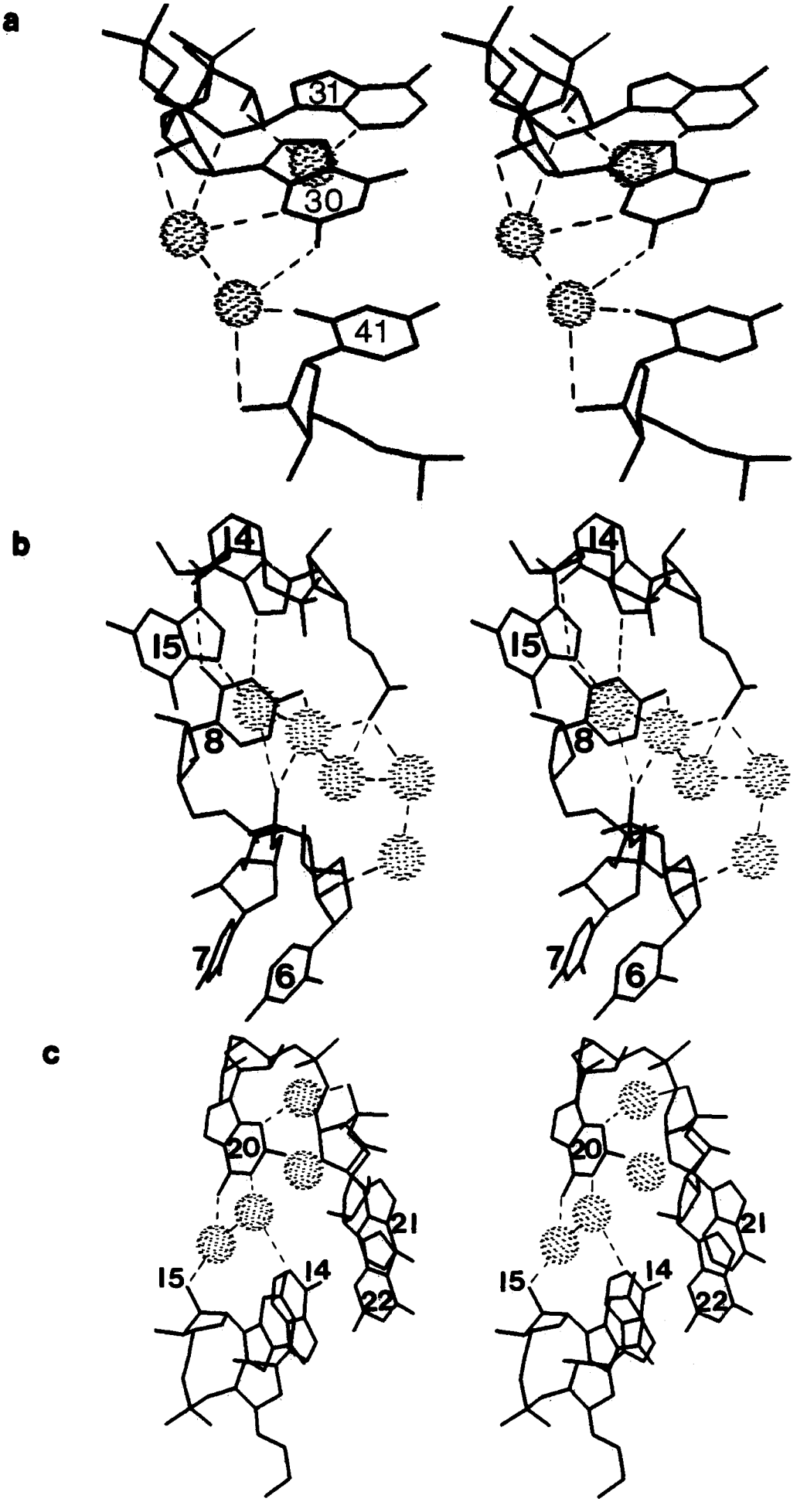
a
31
30
41
b
14
15
8
7
6
c
20
21
15
14
22

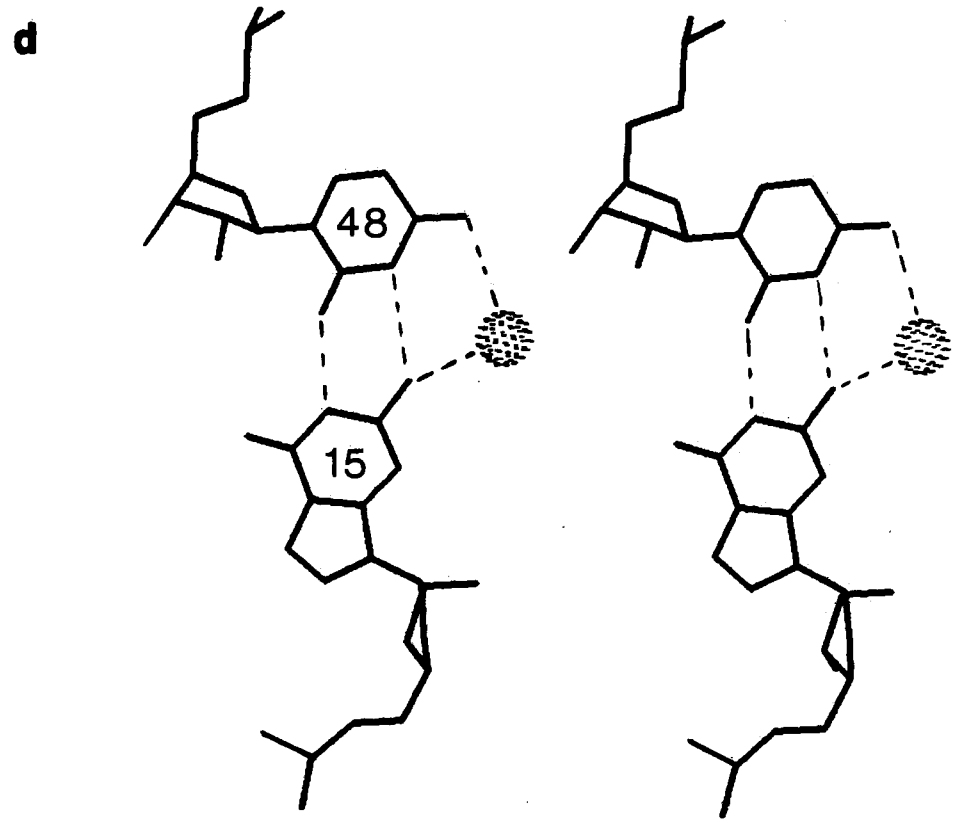

FIGURE 4: (a) Stereoview of the partial hydration around A31 and G30 and U41. (b) Stereoview of the partial hydration around the invariant reversed Hoogsteen base pair U8-A14. (c) Stereoview of the partial hydration around G20. (d) Stereoview of the G15-C48 base pair with a water molecule bridging the two bases.

of the ribose sugars to the N3 of purines or the O2 of pyrimidines. Depending on the neighboring base pairs, such water molecules interact with other water molecules, themselves hydrogen bonded to an adjacent base, thereby stabilizing the base pairing. This is especially the case with unusual base pairing, like the wobble G-U pair, because those pairs, due to their relative reorientation with respect to the usual Watson–Crick pairs, shape an internal cavity into which water molecules can fit. As a rule, each cavity formed by the polynucleotide fold is filled by one or more water molecules. This is illustrated by Figure 4b, which displays a partial view of the hydration around the bend following U7 and the invariant base pair U8-A14. At least five water molecules buffer the close approach of the phosphate groups of U7 and A14. The water bridging O4 of U8 to O1P of A14 and O2P of U7 was found in the other two tRNA structures. Interestingly, all these water molecules fill the site in which ethidium bromide was found after its diffusion into crystals of yeast tRNA^{Phe} (Liebman et al., 1977). Thus, they would have to be displaced to allow ethidium bromide binding, a very similar situation to the displacement of the spine of hydration out of the minor groove of B-DNA upon netropsin binding (Kopka et al., 1985). Another complex interaction, which was also partially seen in the orthorhombic form of yeast tRNA^{Phe}, is shown in Figure 4c. A water molecule bridges the O(2′) of G15 with the O6 of G20, while another bridges the N1 atoms of A14 and G20.

The way a water molecule can stabilize an unusual base pair is displayed in Figure 4d for the trans Watson–Crick G15-C48, or Levitt pair (Levitt, 1969), between which a water molecule bridges N2 of G15 to N4 of C48. There are several methyl groups in yeast tRNA^{Phe}, and they seem to have a tendency to attract water molecules. Two examples are shown in Figure 5. Water molecules also form intermolecular bridges between symmetry-related tRNA molecules, although those are not numerous in the monoclinic form of yeast tRNA^{Phe} due to the reduced number of packing contacts. An example is shown in Figure S-6: a water molecule bridges O2 of C13 to O4 of D17 of a symmetry-related molecule, and another water bridges N1 of A14 to O6 of G19 of a second symmetry-related molecule. There is also a hydrogen bond between these two symmetry-related molecules: between O(2′) of D17 and an anionic oxygen of G19.

Magnesium and Heavy Atom Binding Sites. Five magnesium binding sites have been identified (Figure 6a). Three are the same as those previously described (Hingerty et al., 1978): one is bound to the P10 loop via water bridges to anionic oxygens of residues U8–U12, the second is directly bound to anionic oxygens of G20 and A21, and the third one is lodged in a cavity between the anionic oxygens of G19, O6 of G20, and O4 of U59. The fourth site determined by Hingerty et al. (1978), linking anionic oxygen atoms of A14 and G57 of symmetry-related molecules, was assigned in the present refinement to a water molecule. The last two magnesium sites are buried inside the major groove of the anticodon stem, one slightly above the anticodon loop and the other below the dihydrouridine stem (see Table S-IV), and both have occupancies of only half. Close to the latter site, a spermine molecule was found in the orthorhombic form (Quigley et al., 1978; Teeter et al., 1980) and in the monoclinic form (Hingerty et al., 1978) of yeast tRNA^{Phe}. The former site is close to a magnesium site, suggested previously (Stout et al., 1978) and similar to the fourth site of yeast tRNA^{Phe} in the orthorhombic form (Sussman et al., 1978; Holbrook et al., 1978; Quigley et al., 1978). In the present refinement, this magnesium site has no direct link to any anionic phosphate oxygen but makes several contacts to the last two base pairs of the anticodon stem and to bases Y37 and A38 of the anticodon loop, while the fourth site of the orthorhombic form

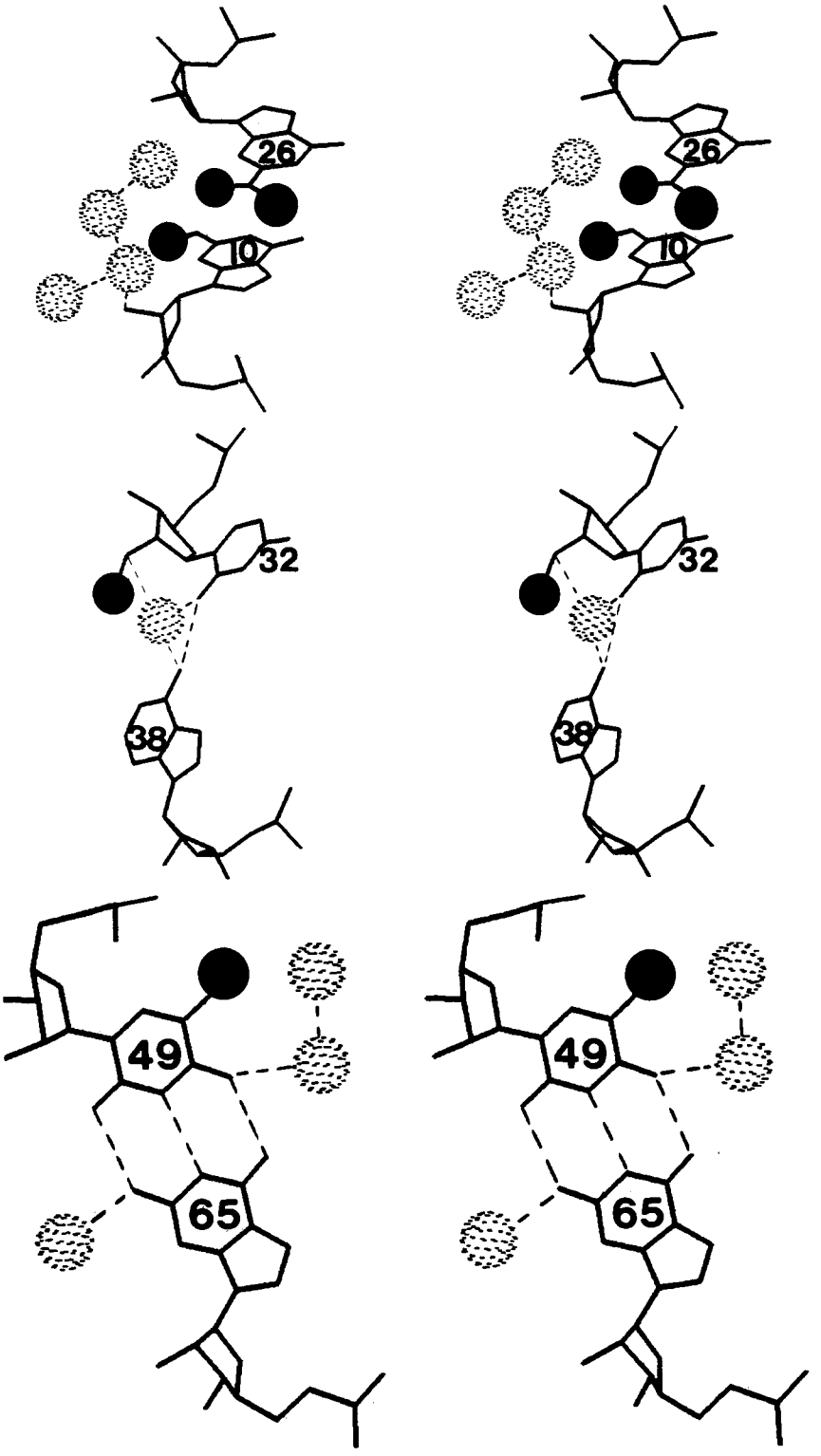

FIGURE 5: Stereoviews of the solvent environment around methyl groups (represented as dark circles).

appeared to be better described as a water molecule bridging the N7 of A36 and Y37. Concerning the fourth site of the orthorhombic form, a similar conclusion was reached by Hingerty et al. (1978) in the monoclinic form of yeast $tRNA^{Phe}$, although they did not find any magnesium ion in the anticodon stem and loop. The last two magnesium sites are shown on Figure 6b and their contacts with the major groove of the anticodon stem in Table V. The water molecules of the hydrated magnesium ions tend to bridge exocyclic groups of successive base pairs in the major groove. A re-refinement (unpublished results) of the orthorhombic form of yeast $tRNA^{Phe}$ shows evidence for of the same two magnesium ions and not for the presence of a spermine. However, at this resolution, it might be difficult to distinguish between the two interpretations.

The interactions of the heavy atom with the tRNA molecule have already been discussed extensively (Jack et al., 1978; Stout et al., 1978). The first lanthanide site (samarium, gadolinium) is the same as the first magnesium site. The second lanthanide site is occupied by a solvent molecule (water or ion). The two major gold sites are displayed in Figure S-7. The first gold site is the same as the first osmium site. The second

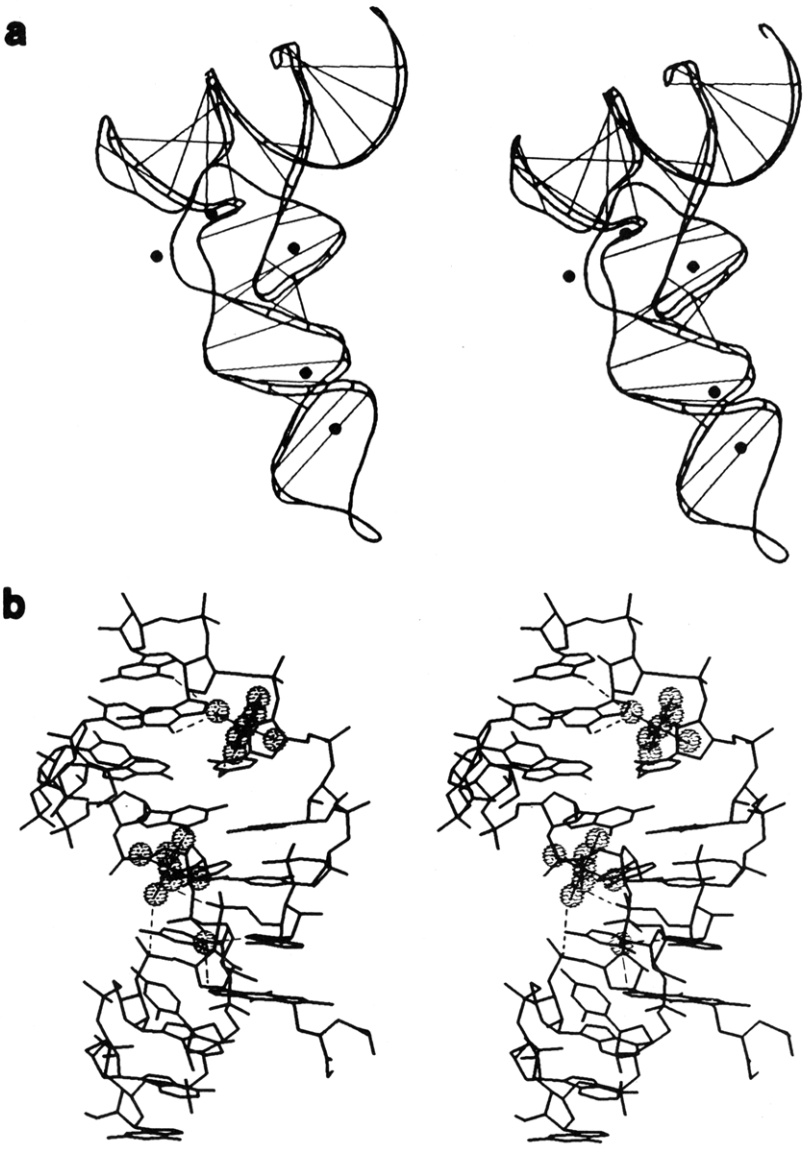

FIGURE 6: (a) Stereoview of the phosphate backbone of tRNA^{Phe} with the five bound magnesium sites. (b) Stereoview of the major groove of the anticodon stem with the two magnesium ions, one bound in the stem and the other in the loop. The solvent site in the anticodon loop that bridges the N7 of A36 and Y37 is also shown. Notice the hydrogen bond between O2 of residue C32 and N6 of residue A38.

gold site is the same as the second osmium site or the unique platinum site of the *trans*-amino Pt derivative. The environments of the various gold sites are given in Table V. Note that the Pt and the Os(2) sites show interactions similar to that of Au(2) and should therefore constitute an energetically favored binding mode. Interestingly, this is similar to the binding of cobalt or nickel derivatives to nucleotides (Swaminathan & Sundaralingam, 1979).

Conclusions

Restrained least-squares refinement of the monoclinic form of yeast tRNA^{Phe} has allowed the determination of atomic temperature factors and group-averaged occupancies, as well as the location of several solvent molecules and five magnesium sites. Temperature factors and occupancies obtained in the present refinement are physically meaningful and allow useful comparisons to be made with the same parameters derived in a similar way for other forms of yeast tRNA^{Phe} or of other tRNAs. Also, confidence in the positions of the solvent molecules has increased since similar interactions were found in either previous refinements (Hingerty et al., 1978; Quigley et al., 1978; Sussman et al., 1978), in re-refinements of yeast tRNA^{Phe} (unpublished results), or in the refinement of yeast tRNA^{Asp} (unpublished results). The new refined coordinates with temperature factors, occupancies, and solvent positions have been deposited with the Brookhaven Data Bank.

Acknowledgments

We gratefully thank Dr. D. Moras, Director of the Laboratoire de Cristallographie Biologique, for the use of the computing and graphics facilities and for his interest and Ph. Dumas for help with the graphics program FRODO. We are grateful to Drs. W. K. Olson and R. E. Dickerson for making available their programs for determining helix parameters.

Supplementary Material Available

Table S-I, giving agreement statistics for geometrical parameters and the σ values used in the refinement; Table S-II, giving the conformational torsion angles of yeast tRNA^{Phe}; Table S-III, giving intramolecular contacts; Table S-IV, giving environments of the water molecules bound to the two magnesium ions in the anticodon stem and of the gold heavy atoms; Figure S-1, showing displacements of the phosphate centers between the three models of tRNA^{Phe}; Figure S-2, showing propeller twist angles for the base pairs of the anticodon, amino

acid, and thymine stems before and after the inclusion of water molecules in the refinement; Figure S-3, showing a stereoview of the sugar–phosphate backbone of yeast $tRNA^{Phe}$ showing the C(2′)-endo sugar puckers; Figure S-4, showing stereoviews of the interaction of A21 with U8-A14 and of the interaction of residues U8-A9 with the major groove of the D stem; Figure S-5, showing stereoviews of the interactions between G18 and G19 of the D loop and P55-G57-C56 of the T loop and of the contacts made by the phosphate of residue C60; Figure S-6, showing a stereoview of two water bridges between symmetry-related tRNA molecules; and Figure S-7, showing a stereoview of the environments of two gold sites (Au1 and Au2) (13 pages). Ordering information is given on any current masthead page.

Registry No. Mg, 7439-95-4; Au, 7440-57-5.

REFERENCES

Altona, C., & Sundaralingam, M. (1972) *J. Am. Chem. Soc. 94*, 8205–8209.

Arnott, S., Hukins, D. W. L., Dover, S. D., Fuller, W., & Hodgson, A. R. (1973) *J. Mol. Biol. 81*, 107–122.

Fratini, A. V., Kopka, M. L., Drew, H., & Dickerson, R. E. (1982) *J. Biol. Chem. 257*, 14686–14707.

Goddard, J. P. (1977) *Prog. Biophys. Mol. Biol. 32*, 233–308.

Hendrickson, W. A, & Konnert, J. H. (1980) in *Biomolecular Structure, Function, Conformation, and Evolution* (Srinivasan, R., Ed.), Vol. I, pp 43–50, Pergamon Press, Oxford.

Hingerty, B., Brown, R. S., & Jack, A. (1978) *J. Mol. Biol. 124*, 523–534.

Holbrook, S. R., Sussman, J. L., Wade-Warrant, R., & Kim, S. H. (1978) *J. Mol. Biol. 123*, 631–660.

Ichikawa, T., & Sundaralingam, M. (1972) *Nature (London) New Biol. 236*, 174–175.

Jack, A., & Levitt, M. (1978) *Acta Crystallogr., Sect. A: Cryst. Phys., Diffr., Theor. Gen. Crystallogr. A34*, 931–935.

Jack, A., Ladner, J. E., Rhodes, D., Brown, R. S., & Klug, A. (1977) *J. Mol. Biol. 111*, 315–328.

Jones, T. A. (1982) in *Computational Crystallography* (Sayre, D., Ed.) pp 303–310, Clarendon Press, Oxford.

Jurnak, F. A., & McPherson, A. (1985) in *Biological Macromolecules and Assemblies*, Vol. 2, Appendix, pp 471–494, Wiley-Interscience, New York.

Kim, S. H., Quigley, G., Suddath, F. L., & Rich, A. (1971) *Proc. Natl. Acad. Sci. U.S.A. 68*, 841–845.

Konnert, J. H., & Hendrickson, W. A. (1980) *Acta Crystallogr., Sect. A: Cryst. Phys., Diffr., Theor. Gen. Crystallogr. A36*, 344–349.

Kopka, M. L., Yoon, C., Goodsell, D., Pjura, P., & Dickerson, R. E. (1985) *Proc. Natl. Acad. Sci. U.S.A. 82*, 1376–1380.

Ladner, J. E., Finch, J. T., Klug, A., & Clark, B. F. C. (1972) *J. Mol. Biol. 72*, 99–101.

Ladner, J. E., Jack, A., Robertus, J. D., Brown, R. S., Rhodes, D., Clark, B. F. C., & Klug, A. (1975) *Proc. Natl. Acad. Sci. U.S.A. 72*, 4414–4418.

Levitt, M. (1969) *Nature (London) 224*, 759–763.

Liebman, M., Rubin, J., & Sundaralingam, M. (1977) *Proc. Natl. Acad. Sci. U.S.A. 74*, 4821–4825.

Mizuno, H., & Sundaralingam, M. (1978) *Nucleic Acids Res. 5*, 4451–4461.

Moras, D., Dock, A. C., Dumas, P., Westhof, E., Romby, P., Ebel, J. P., & Giege, R. (1986) *Proc. Natl. Acad. Sci. U.S.A.* (in press).

Quigley, G. J., & Rich, A. (1976) *Science (Washington, D.C.) 194*, 796–806.

Quigley, G. J., Teeter, N. M., & Rich, A. (1978) *Proc. Natl. Acad. Sci. U.S.A. 75*, 64–68.

Rhodes, D. (1977) *Eur. J. Biochem. 81*, 91–101.

Shakked, Z., Rabinovitch, D., Kennard, O., & Viswamitra, M. A. (1983) *J. Mol. Biol. 166*, 183–201.

Stout, C. D., Mizuno, H., Rao, S. T., Swaminathan, P., Rubin, J., Brennan, T., & Sundaralingam, M. (1978) *Acta Crystallogr., Sect. B: Struct. Crystallogr. Cryst. Chem. B34*, 1529–1544.

Sundaralingam, M. (1969) *Biopolymers 7*, 821–860.

Sundaralingam, M. (1973) in *Conformation of Biological Molecules and Polymers* (Bergman, E. D., & Pullman, B., Eds.) pp 417–455, Academic Press, New York.

Sussman, J. L., Holbrook, S. R., Church, G. M., & Kim, S. H. (1977) *Acta Crystallogr., Sect. A: Cryst. Phys., Diffr., Theor. Gen. Crystallogr. A33*, 800–804.

Sussman, J. L., Holbrook, S. R., Wade-Warrant, R., Church, G. M., & Kim, S. H. (1978) *J. Mol. Biol. 123*, 607–630.

Swaminathan, V., & Sundaralingam, M. (1979) *CRC Crit. Rev. Biochem. 6*, 245–336.

Teeter, M. M., Quigley, G. J., & Rich, A. (1980) in *Nucleic Acid–Metal Ion Interactions* (Spiro, T. G., Ed.) pp 145–177, Wiley-Interscience, New York.

Westhof, E., & Sundaralingam, M. (1983) in *Structure and Dynamics: Nucleic Acids and Proteins* (Clementi, E., & Sarma, R. H., Eds.) pp 135–147, Adenine Press, New York.

Westhof, E., Dumas, P., & Moras, D. (1985) *J. Mol. Biol. 184*, 119–145.

Wintermeyer, W., & Zachau, H. G. (1973) *Biochim. Biophys. Acta 299*, 82–90.